SPECIAL TOPIC — International Conference on Nanoscience & Technology, China 2013

High refractive index sensitivity sensing in gold nanoslit arrays*

Yuan Jun(袁 浚)[a], Kan Qiang(阚 强)[a]†, Geng Zhao-Xin(耿照新)[a,b], Xie Yi-Yang(解意洋)[a], Wang Chun-Xia(王春霞)[a], and Chen Hong-Da(陈弘达)[a]

[a] State Key Laboratory of Integrated Optoelectronics, Institute of Semiconductors, Chinese Academy of Sciences, Beijing 100083, China
[b] School of Information Engineering, Minzu University of China, Beijing 100081, China

(Received 4 September 2013; revised manuscript received 16 December 2013; published online 10 June 2014)

The extraordinary optical transmission (EOT) phenomenon of nano-periodic aperture array in metallic film has been widely investigated and used in biosensors. The surface plasmon resonance and cavity mode in some periodic nanostructures, such as nanohole and nanoslit, cause EOTs at certain wavelengths. This resonance wavelength is sensitive to the refractive index on the surface of periodic nanostructures. Therefore, the metallic nanostructures are expected to be good sensing elements. The sensing performances of gold nanoslit arrays are experimentally and theoretically investigated. Three-dimensional finite difference time domain (FDTD) simulations are utilized to explore their transmission spectra and steady-state field intensity distributions. The electron beam evaporation, electron beam lithography, and ion milling are applied to the gold nanoslit arrays with different widths and periods. The sensing performances of the gold nanoslit array are characterized via transmission spectra in four kinds of refractive index samples. The highest sensitivity reaches 726 nm/RIU when the width of the gold nanoslit array is 38.5 nm.

Keywords: sensors, extraordinary optical transmission, nanoslit array, cavity mode

PACS: 42.81.Pa, 42.25.Bs, 81.16.Rf, 42.65.Yj **DOI:** 10.1088/1674-1056/23/8/084201

1. Introduction

Since 1998, when Ebbesen *et al.* first reported the extraordinary optical transmission (EOT) phenomenon of light through the thin metal film with periodical nanoscale arrays,[1] much effort has been made to explain the unique phenomenon. For example, it has been proved theoretically and experimentally that the surface plasmon resonance (SPR) and cavity mode are the main reasons for EOT.[2–5] The SPR and cavity mode can be supported by a periodic metal nanoslit array when they are irradiated with a transverse magnetic (TM) optical wave at a specific wavelength. Meanwhile, the confined electronic field can be excited at the interface between the metal nanostructure and the supstructure. The resonant spectra of the SPR and cavity mode sensitively vary with the structure parameter of metal arrays and the refractive index environment around the metal arrays.

Owing to the fact that the transmission spectra of metal nano-arrays are sensitive to the change of the refractive index of the environment, researchers have developed and optimized some metal nano-array sensors with different structures.[6–8] Compared with the traditional SPR sensor chip, the metal nano-array sensors can not only real-time monitor the label-free analyte but also significantly reduce the interrogation volumes. This type of biosensor integrated with microfluidics can also minimize the volumes of required detective analyte. Therefore, they are widely used in chemical and biological sensors.[9–12] However, many high-sensitivity sensors with complex structures are difficult to fabricate. It costs much less time and money to fabricate nanoslit arrays than other complex structures by electron beam lithography (EBL). Meanwhile, the coaxial optical path measurement setup of the nanoslit array sensor is simpler than the SPR sensor. In addition, the cavity mode of the nanoslit array with exciting large electric field intensity in the slit has a higher sensitivity. Therefore, the nanoslit array sensor with high sensitivity and a simple structure is a better choice for practical applications.

The purpose of our research is to optimize the structure parameters of gold nanoslit arrays, and improve the sensitivity of the sensor based on the gold nanoslit array. The geometric design on the sensing properties of the gold nanoslit array is investigated by theoretical analysis and numerical simulation. The higher sensitivity of the sensor will be obtained with suitable parameters of the nanoslit array. Besides, the analysis of the experimental result suggests future work on improving the sensitivity of nanoslit array.

2. Fabrication and testing

Gold nanoslit arrays were fabricated by the following processes. (i) A quartz glass (2 cm×2 cm) was cleaned through the standard clean of the semiconductor fabrication process. (ii) 5-nm Ti (adhesive layer) and 90-nm Au were successively

*Project supported by the National Key Basic Research Program of China (973 Program) (Grant Nos. 2011CB933102, 2010CB934104, and 2011CB933203), the National Natural Science Foundation of China (Grant Nos. 61036009 and 61378058), and the Science Innovation Foundation of the Cooperation Project between Jilin Province and Chinese Academy of Sciences (Grant No. 2012CJT0037).

†Corresponding author. E-mail: kanqiang@semi.ac.cn

© 2014 Chinese Physical Society and IOP Publishing Ltd

deposited on the chip by electron beam evaporation. (iii) A 330-nm thick Zep520 resist was spin-coated on the chip. (iv) Electron beam lithography (EBL) was used to pattern different sizes and shapes of nanoslit arrays on the Zep520 resist layer. (v) The patterns were transferred onto the gold film using ion milling. (vi) The Zep520 layer was removed in acetone with an ultrasonic clean of the surface of the sensor chip. (vii) The quartz glass with a metal nanoslit and polydimethylsiloxane (PDMS) with a microchannel were treated with oxygen plasma and bonded together. So the PDMS microfluidic flow cell with our sample is easy to inject the fluids.

Figure 1 shows the measurement setup, which consists of a light source, collimator, polarizer, mirror, objective, beam splitter, CCD, spectrometer, and computer. The testing theory or processes are simply described below. A light beam from a broadband tungsten halogen source (Ocean Optics HL-2000) is collimated by a collimator, and the polarization along the periodic direction of the gold nanoslit array was controlled by a Glan–Taylor polarizer. The light beam normally illuminating the gold nanoslit array sample, which is placed on a stage allowing micron-resolved displacement, excites the SPR and cavity mode on the sample, and two long-working-distance 10× objectives are used to focus the incident light beam on the sample and collect the transmitted signal, respectively. Then the light beam is split by a splitter, and detected by a CCD camera and the spectrometer respectively. Through the CCD camera, the location and focus of the sample can be monitored. A computer analyzes the data from the spectrometer.

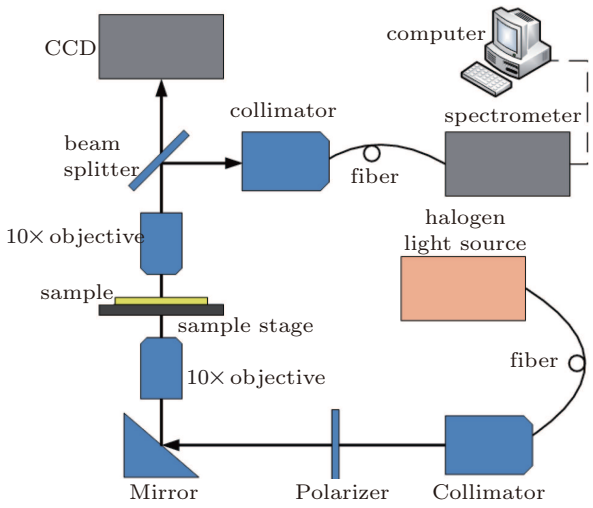


Fig. 1. (color online) Schematic diagram of the transmission spectrum measurement setup.

To examine the sensitivity of the sensor chip, the transmission spectra were recorded when the surface of the sensor chip was covered by four fluids (water, ethanol, glycol, and glycerol) with different refractive indices. The refractive indices of water, ethanol, glycol, and glycerol are 1.333, 1.363, 1.434, and 1.473, respectively.

3. Results and discussion

Comprehensive simulation is used to explore the transmission spectra of gold nanoslit arrays by changing the period p, width of gap w, and refractive index of medium n, and to obtain the suitable structure parameters of the gold nanoslit array sensor. The thickness value of the gold film is kept at 90 nm in simulation and experiment, because the cavity mode could not be the main factor of EOT when the gold film is very thin.[5,13,14] The intensity of the electronic field at the interface is evanescent along the direction normal to the interface, both electronic fields on the two sides of the gold film rarely couple with each other when the thickness value of the gold film is 90 nm.[5,15]

Simulations are carried out using a finite difference time domain (FDTD) software code developed by Lumerical Solutions, Inc. The FDTD calculations are used for p from 600 nm to 700 nm, and w from 30 nm to 110 nm. A fit to experimental values is used to model the dispersive Au film.[16] The refractive index of the quartz substrate is 1.455. The simulation domain used the perfectly matched layer boundary conditions above and below the structure to prevent reflections and anti-symmetric boundary conditions to determine the periodicity of the array. With polarization along the periodicity direction, a plane wave source is normally incident on the nanoslit array. A frequency domain profile monitor collects the transmission spectrum through the nanoslit array. The refractive index sensing sensitivity is determined by the characteristic change of transmission spectrum via changing the refractive index of the solution around the gold nanoslit array.

In Fig. 2(a), calculation transmission spectra of gold nanoslit arrays ($p = 700$ nm and $w = 50$ nm) in different fluids show that between the wavelengths of 500 nm and 1100 nm, there are three main transmission peaks of the gold nanoslit array, which shift toward longer wavelengths with increasing n. The peaks in ranges from 1030 nm to 1080 nm and from 630 nm to 680 nm are the SPP-BW 1 and 2 order mode peaks, respectively, and the peaks in a range from 920 nm to 1020 nm are the cavity mode peaks.[17,18] The three transmission peaks demonstrate different sensing sensitivities of refractive index S ($S = \Delta\lambda/\Delta n$, $\Delta\lambda$ is the wavelength shift of transmission peak with the change in the refractive index of medium Δn). The values of S of SPP-BW 1 and 2 order mode peaks and the cavity mode peak are 211, 202, and 760 nm/RIU (Fig. 2(b)), respectively. Figures 2(c) and 2(d) show the calculated steady-state time-averaged total electric field intensities of the gap cross section at the resonance wavelength in water and glycerol respectively. The electric field intensity in glycerol is stronger than that in water, so the amplitude of the cavity mode peak in glycerol is much larger. Those phenomena originate from the refractive index of the medium close to the substrate.[5,19] Both figures 2(c) and 2(d) also show that the electric field of the cavity mode is localized in the gap, therefore, the value of S of the cavity mode peak is high. Then we calculate the cavity mode peak by changing the parameter of the gold nanoslit array. The S of the sensor will be improved when the parameters of the sensor are suitable.

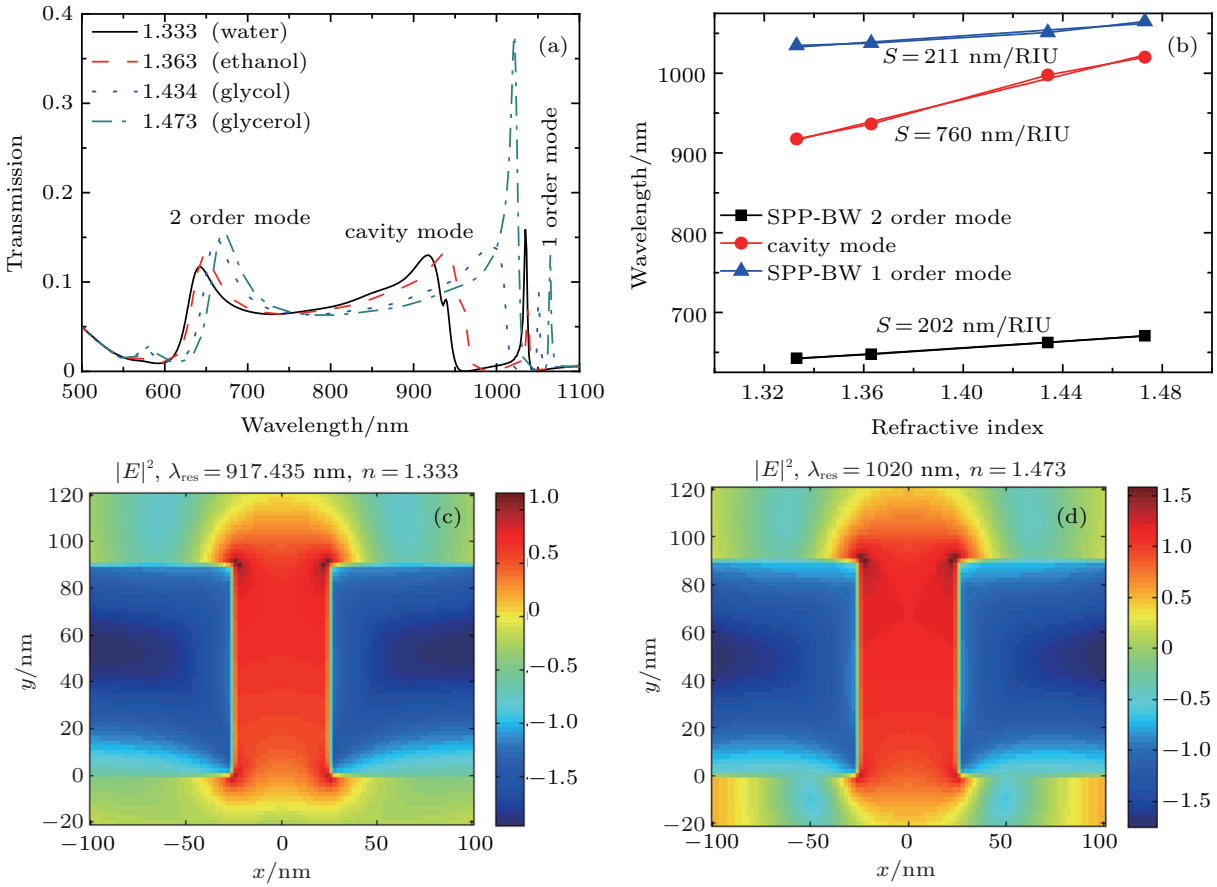


Fig. 2. (color online) Simulation results of the optical properties of a nanoslit array with $p = 700$ nm and $w = 50$ nm by FDTD. (a) The transmission spectra of the nanoslit array in fluids with different values of n. The three wavelengths of the transmission peaks are red shifted with n increasing. (b) Linear fitting between the wavelength of the transmission peak and n. The S of the cavity mode and SPP-BW 1 order and 2 order mode are 760, 211, and 202 nm/RIU, respectively. The S of the cavity mode is the highest. (c) and (d) log 10-scale plots of the electric field intensity in water and glycerol of a cross section of the nanoslit when the cavity mode is excited. Note the different color bars; the electric field intensity in glycerol is much stronger than that in water.

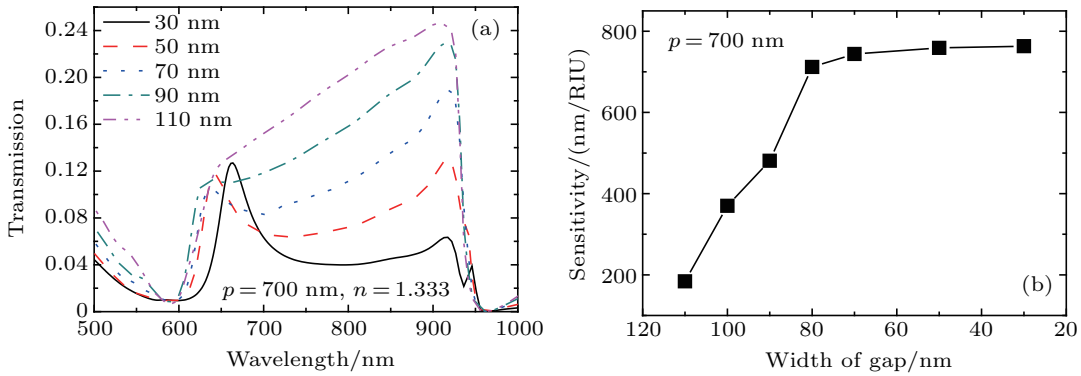


Fig. 3. (color online) (a) Variations of calculated transmission spectra of a gold nanoslit array with wavelength w. Other parameters are $p = 700$ nm and $n = 1.333$. (b) Calculated value of S versus w when p is 700 nm.

First, the transmission spectra are simulated by keeping $p = 700$ nm and changing w from 30 nm to 120 nm in different values of n. Figure 3(a) shows the transmission spectra of a nanoslit array with different values of w in water ($n = 1.333$). With w changing from 30 nm to 110 nm, the amplitude of the cavity mode peak is increasing and the wavelength is slightly blue shifted. In Fig. 3(b), the value of S increases as the value of w deceases. Note that S approaches to saturation as w is smaller than 70 nm, this is a result of the intensity of the localized electric field becoming slightly stronger when w ($w \leq 70$ nm) decreases.

Then, the transmission spectra are simulated via keeping w at 50 nm and changing p from 600 nm to 700 nm for different values of n. In Fig. 4(a), for the transmission spectra of a nanoslit array with different values of p in water, the wavelength of the cavity mode transmission peak is red shifted, but the amplitude is almost invariant. Figures 3(a) and 4(a) show that the resonance wavelength mostly depends on p and the amplitude on w. The values of S for different p nanoslit arrays are demonstrated in Fig. 4(b), and it is almost linearly proportional to p.

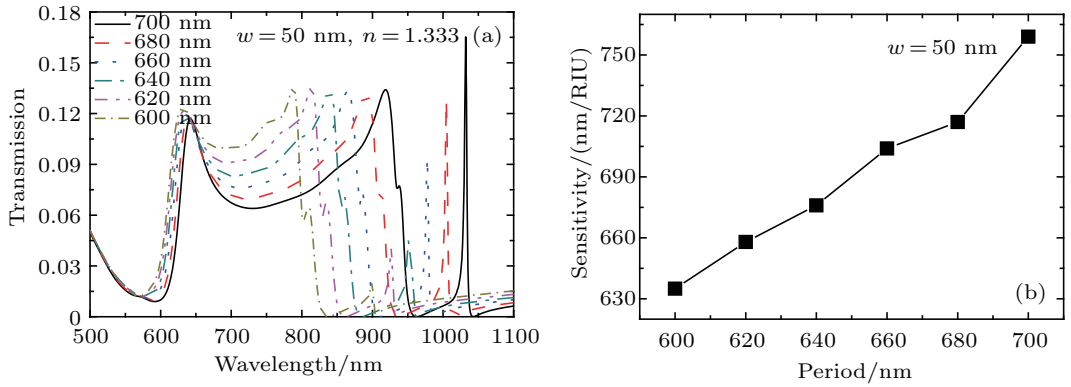


Fig. 4. (color online) Calculated transmission spectra of a nanoslit array for different values of p. Other parameters are $w = 50$ nm and $n = 1.333$. (b) Calculated S versus p when w is 50 nm.

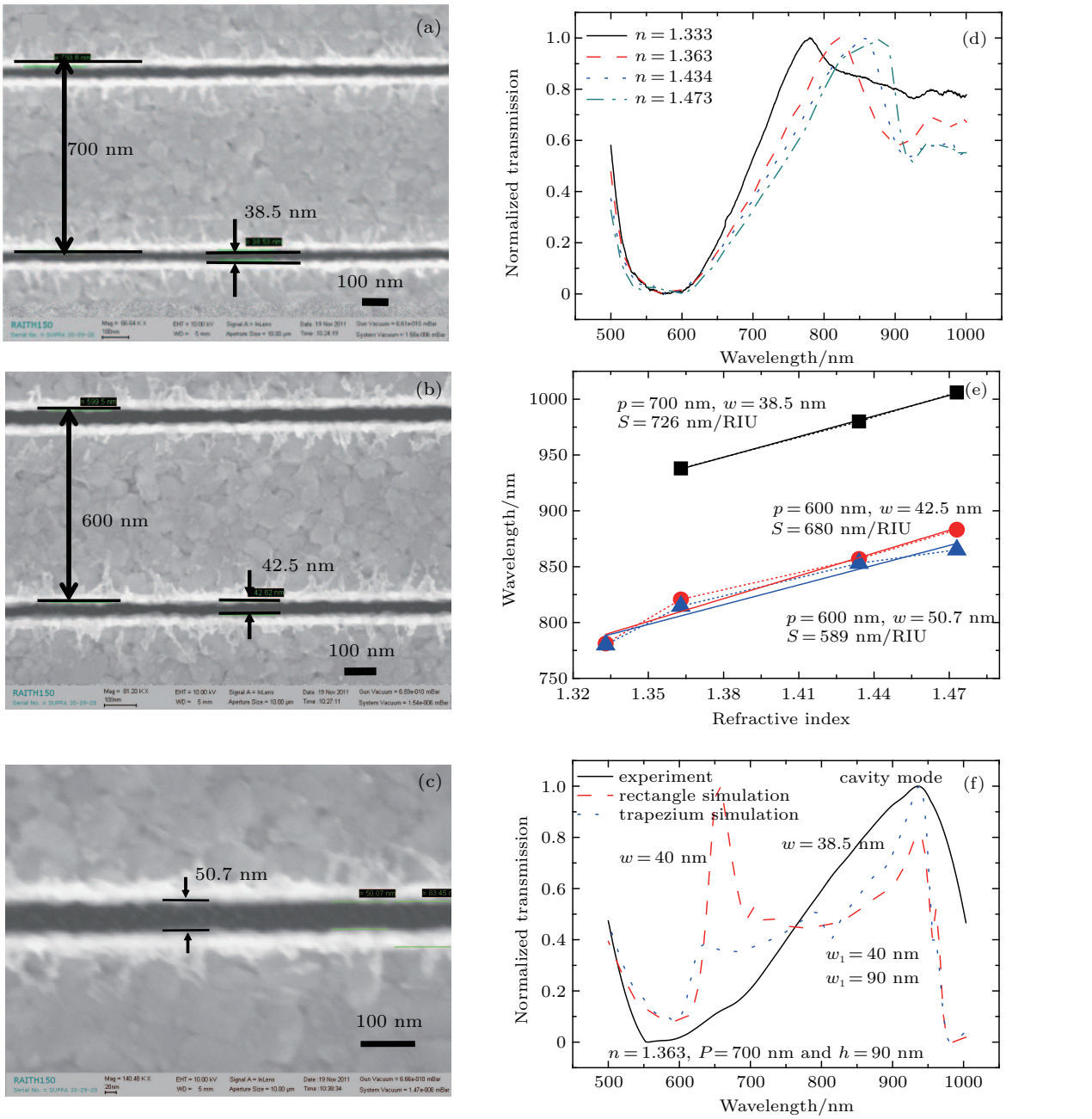


Fig. 5. (color online) (a)–(c), SEM images of three different nanoslit arrays. The gold film is 90-nm thick, (a) $p = 700$ nm, $w = 38.5$ nm, (b) $p = 600$ nm, $w = 42.5$ nm, and (c) $p = 600$ nm, $w = 50.7$ nm. (d) The measurement transmission spectra of a nanoslit array with $p = 600$ nm and $w = 42.5$ nm in fluids with different values of n. The transmission peak of the cavity mode is red shifted with the value of n increasing. The transmission spectra are normalized. (e) Linear fitting between the wavelengths of transmission peaks and n. The value of S of gold nanoslit arrays in panels (a), (b), and (c) are 726, 680, and 589 nm/RIU, respectively. (f) The transmission spectra of measurement and simulation with rectangle and trapezium shaped gaps. It shows that the actual gap is closer to a trapezium than a rectangle.

According to the results of the simulation, the gold nanoslit arrays with different values of p and w are fabricated. Figures 5(a)–5(c) show the SEM images of three nanoslit arrays ((a) $p = 700$ nm, $w = 38.5$ nm, (b) $p = 600$ nm, $w = 42.5$ nm, (c) $p = 600$ nm, $w = 50.7$ nm). Then their transmission spectra in different fluids are measured. Figure 5(d) shows the transmission spectra of the structure in Fig. 5(b), and all the spectra are normalized. Obviously, the wavelength of the cavity mode transmission peak is red shifted as n increases. In Fig. 5(e), the values of S for the three structures in Figs. 5(a)–5(c) are 726, 680, and 589 nm/RIU, respectively. The value of S of 726 nm/RIU is higher than those of previously reported nano-arrays.[20,21] Meanwhile, the values of n range from 1.333 to 1.473 for the gold nanoslit arrays in Figs. 5(b) and 5(c), and they are also larger than those of previously reported nanoperiod arrays.[12] Comparing the measurement results with the simulation results, the measurement value of S shows that they are in good agreement with the simulation one at a qualitative level, and it is about 30 nm/RIU which is less than the simulation value. In fact, errors exist for all samples we fabricated. This is not surprising, because of the rough surface of gold film and the trapezium cross section of the gap that is not an ideal rectangle but a trapezium, whose top side is a little larger than the bottom side. This results from the fabrication process, such as Au ion milling.[22] Figure 5(f) shows three normalized transmission spectra in ethanol solution ($n = 1.363$). The solid one is the measurement transmission spectrum of the structure in Fig. 5(b), and the spectra (dashed and dotted) are the simulation results of an ideal rectangle ($w = 40$) and a trapezium (the width of the top side is 90 nm and the bottom side is 40 nm), respectively. Because the top side is wider, the amplitude of the SPP-BW 2 order mode peak becomes smaller than the cavity mode and disappears in the measurement spectrum. However, the wavelength of the cavity mode is varied little, so the measurement S of the cavity mode is in good agreement with the simulation value.

The values of S of the fabricated sensors are high, but the properties of gold nanoslit arrays refractive index sensor could be optimized to obtain a higher value of S. Now two potential approaches are under investigation. The first one is to improve the reliability of the fabrication process, which makes more precise and integrated nanostructures.[8] The second one is to design new nanostructures with a unique sensing property.[23,24]

4. Conclusion

In this paper, the performances of gold nanoslit arrays are simulated and experimentally investigated. The results show that the cavity mode transmission peaks of the gold nanoslit array shift toward longer wavelengths with increasing the environment refractive index, and the gold nanoslit array is demonstrated to be a good sensing element. Geometrical investigation results of gold nanoslit arrays show that the sensitivity approaches to saturation as the width of the nanoslit is smaller than 70 nm and is almost linearly proportional to the period when the width is unchanged. Meanwhile, we fabricated and measured several gold nanoslit arrays with different periods and widths. The highest sensitivity of 726 nm/RIU is obtained from the structure with a period of 700 nm and a width of 38.5 nm. Comparing the simulation results with the measurement results, the measurement results show that they are in good agreement with the simulation results. Based on the above study, gold nanoslit arrays with simple structure show high sensitivities. So the gold nanoslit arrays have a bright future to be widely used in sensing applications, owing to their high sensitivity, fast fabrication, convenient integration, and small size.

References

[1] Ebbesen T W, Lezec H J, Ghaemi H F, Thio T and Wolff P A 1998 *Nature* **391** 667
[2] Ruan Z and Qiu M 2006 *Phys. Rev. Lett.* **96** 233901
[3] Liu H T and Lalanne P 2008 *Nature* **425** 728
[4] Pitarke J M, Silkin V M, Chulkov E V and Echenique P M 2007 *Rep. Prog. Phys.* **70** 1
[5] Garcia-Vidal F J, Martin-Moreno L, Ebbesen T W and L Kuipers 2010 *Rev. Mod. Phys.* **82** 729
[6] Yanik A A, Cetin A E, Huang M, Artar A, Mousavi S H, Khanikaev A, Connor J H, Shvets G and Altug H 2011 *Proc. Natl. Acad. Sci.* **108** 11784
[7] Li J H, Kan Q, Wang C X and Chen H D 2011 *Chin. Opt. Lett.* **9** 090501
[8] Jose J, Jordan L R, Johnson T W, Lee S H, Wittenberg N J and Oh S H 2013 *Adv. Funct. Mater.* **23** 2812
[9] Haes A J, Hall W P, Chang L, Klein W L and Van Duyne R P 2004 *Nano Lett.* **4** 1029
[10] Gan Q Q and Bartoli F J 2009 *Opt. Lett.* **34** 2180
[11] Zhao H J 2012 *Chin. Phys. B* **21** 087104
[12] Jia P P, Jiang H, Sabarinathan J and Yang J 2013 *Nanotechnology* **24** 195501
[13] Yoon J W, Jung M J, Song S H and Magnusson R 2012 *IEEE J. Quantum Electron.* **48** 852
[14] Rahman A T M A, Majewski P and Vasilev 2012 *Opt. Lett.* **37** 1742
[15] Pacifici D, Lezec H J, Atwater H A and Weiner J 2008 *Phys. Rev. B* **77** 115411
[16] Lide D R 2004 *CRC Handbook of Chemistry and Physics* (Boca Raton: CRC Press) ISBN 0-8493-0485-7
[17] Weiner J 2009 *Rep. Prog. Phys.* **72** 064401
[18] Chang S H, Gray S K and Schatz G C 2005 *Opt. Express* **13** 3150
[19] Tellez G A C, Hassan S, Tait R N, Berini P and Gordon R 2013 *Lab on a Chip* **13** 2541
[20] Henzie J, Lee M H and Odom T W 2007 *Nat. Nanotechnol.* **2** 549
[21] Sharpe J C, Mitchell J S, Lin L, Sedoglavich N and Balaikie R J 2008 *Anal. Chem.* **80** 2244
[22] Zhang J Y, Wang X F, Wang X D, Fan Z C, Li Y, Ji A and Yang F H 2010 *Nanotechnology* **21** 075303
[23] Huang L L, Chen X Z, Bai B F, Tan Q F, Jin G F, Zentgraf T and Zhang S 2013 *Light: Science & Applications* **2** 70
[24] Halas N J, Lal S, Chang W S, Link S and Nordlander P 2011 *Chem. Rev.* **111** 3913